W. H. Chang
H. S. Lee

Potential Distribution of an Inhomogeneously Doped MIS Array

Abstract: A numerical method is used to obtain the potential distribution of a two-dimensional, inhomogeneously doped MIS array under pulse voltage operation. The effects of interface charge and of impurity doping and its locations on the surface potential profile are presented. The technique is useful for designing an appropriate surface potential profile for ion-implanted charge-coupled devices.

Introduction

In an ion-implanted charge-coupled device [1], the minority carriers are moved along the silicon surface by potential wells formed by MIS (metal-insulator-semiconductor) capacitors with the substrate nonuniformly doped along the surface. When the surface potential profile is properly designed, a heavily ion-implanted region prevents the carriers from moving backward, so that information can be transformed unidirectionally. The effectiveness of such a barrier and the transfer speed of the device depend critically on the surface potential distribution. The potential distributions of several semiconductor devices have been studied [2–5]. However, these analyses were limited to either a junction FET device or a MOSFET (metal-oxide-semiconductor field-effect-transistor) device with uniformly doped substrate.

The present paper describes a numerical technique to study the two-dimension potential and charge distribution of an MIS array. Using a Green's function, the finite-difference method can be applied only to the silicon region. Using the conventional procedure, the finite-difference method is applied both to the silicon region and to the oxide region. With the Green's function, various electrode shapes, oxide thicknesses and electrode gaps can be analyzed using the same computer program. Furthermore, this approach can be easily extended to analyze the time-dependent charge transfer phenomenon, but this topic is reserved for a future paper. The technique is useful for designing an appropriate surface potential profile for ion-implanted charge-coupled devices. Results are obtained that show the effects on the surface potential distribution due to surface charges, relative location of the highly doped implanted region under the electrode, and substrate doping in the interelectrode region.

Mathematical model

Consider a general n-electrode MIS array, as shown in Fig. 1. The ith electrode has width W_i^* and is located a distance h_i^* above the silicon surface. (The superscript * indicates an unnormalized quantity.) The upper and lower half-spaces are filled with SiO_2 and silicon, respectively. For convenience, the bulk substrate is assumed to be p-type and to be doped to a density N_{AB}^*. The ion-implanted or deffused region has a dopant density $N_A^*(x^*, y^*)$. When positive voltage pulses are applied to the electrodes, the silicon surface is depleted. The time constant associated with the transport of the majority

Figure 1 MIS array with nonuniformly doped substrate.

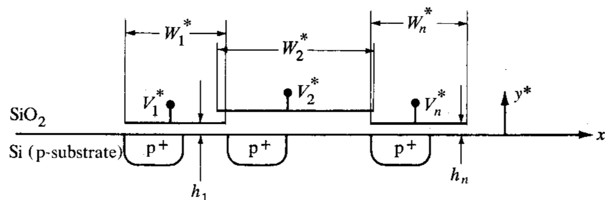

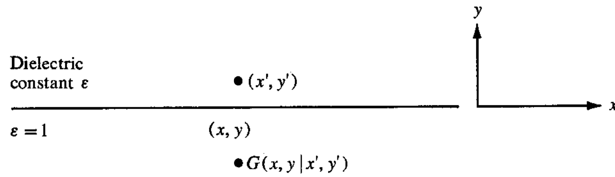

Figure 2 Potential at (x, y) due to a line charge at (x', y').

carriers is the dielectric relaxation time of the substrate, typically on the order of 10^{-11} s for a 10-Ω-cm p-type silicon substrate [6], so the majority carriers are able to follow the applied voltages and are in quasi-equilibrium at all times. The time constants associated with the supply of the minority carriers by diffusion and generation-recombination processes in the depletion region, however, are much longer compared to that of the applied voltage pulse. Thus, the minority carriers in the original well remain unchanged both in magnitude and position after the voltages have been applied. Since the majority carriers are always in equilibrium (to a first approximation), there is no hole current in the substrate. Therefore, from the continuity equation for hole current,

$$\mathbf{J}_p^*(x^*, y^*) = -qD_p \nabla p^* - q\mu_p p^* \nabla \phi^* = 0, \tag{1}$$

and the Einstein relation,

$$D_p = \mu_p \frac{kT}{q}, \tag{2}$$

the hole density in the substrate becomes

$$P^*(x^*, y^*) = p_0^* e^{-\frac{q\phi^*}{kT}}, \tag{3}$$

where q is the magnitude of the electronic charge, D_p the hole diffusion coefficient, μ_p the hole mobility, k the Boltzman constant, T the temperature, and p_0^* a constant. The total charge density $\rho^*(x^*, y^*)$ in the silicon is the sum of the holes $p^*(x^*, y^*)$, electrons $n^*(x^*, y^*)$, and ionized impurity atoms $N_A^*(x^*, y^*)$, or

$$\rho^*(x^*, y^*) = q[p^*(x^*, y^*) - n^*(x^*, y^*) - N_A^*(x^*, y^*)]. \tag{4}$$

The impurity atoms are assumed to be fully ionized, and $N_A^*(x^*, y^*) = N_{AB}^*$ in the bulk substrate. Further simplification is made by assuming that the electron density, except for the externally injected electrons $N_e^*(x^*)$, is small compared to the density of ionized impurity atoms. This simplification is a good assumption because the electron density is given approximately by $n_i^1/N_A^*(x^*, y^*)$, where n_i is the intrinsic carrier concentration; this is much smaller than $N_A^*(x^*, y^*)$. Furthermore, far from the surface, the substrate must be neutral. If we neglect the electron density, p_0^* is then given by N_{AB}^*. The total charge density (4) becomes

$$\rho^*(x^*, y^*) = q[N_{AB}^* e^{-\frac{q\phi^*}{kT}} - N_A^*(x^*, y^*)] + \delta(y^*)\, q[N_S^*(x^*) - N_e^*(x^*)], \tag{5}$$

where the effective immobile surface charge density $N_S^*(x^*)$ and the injected electron density $N_e^*(x^*)$ are included. They are assumed to be confined to the silicon surface with infinitesimal thickness. The function $\delta(y^*)$ is the Dirac delta function.

The potential $\phi^*(x^*, y^*)$ satisfies the Laplace and Poisson equations in the upper and lower half-spaces, respectively; i.e.,

$$\nabla^2 \phi^* = 0, \qquad y^* \geq 0; \tag{6}$$

$$\nabla^2 \phi^* = -\rho^*(x^*, y^*)/\varepsilon_{Si}^*, \qquad y^* \leq 0, \tag{7}$$

with the boundary conditions,

$$\phi^* = V_i^{*\prime} = V_i^* - \phi_{MS}^* \text{ on the } i\text{th electrode}; \tag{8}$$

$$\phi^* \to 0 \text{ as } (x^{*2} + y^{*2})^{\frac{1}{2}} \to \infty, \tag{9}$$

where V_i^* is the applied voltage on the ith electrode and ϕ_{MS}^* is the work function difference between the metal and the bulk silicon substrate.

The permittivities of silicon and oxide are ε_{Si}^* and ε_{Ox}, respectively. No space charge is assumed to exist in the oxide. On the silicon-oxide boundary, the potential and the tangential electric field are continuous; the normal electric field is discontinuous by

$$\varepsilon_{Ox}^* \frac{\partial \phi^*}{\partial y^*}\bigg|_{y^*=0+} - \varepsilon_{Si}^* \frac{\partial \phi^*}{\partial y^*}\bigg|_{y^*=0-} = -q[N_S^*(x^*) - N_e^*(x^*)]. \tag{10}$$

By defining the following normalized quantities,

$$\lambda_D = \left(\frac{\varepsilon_{Si}^* kT}{q^2 N_{AB}^*}\right)^{\frac{1}{2}}; \qquad x = \frac{x^*}{\lambda_D}; \qquad y = \frac{y^*}{\lambda_D};$$

$$\phi = \phi^* kT/q; \; V_i' = \frac{V_i'^*}{kT/q};$$

$$N_A(x, y) = \frac{N_A^*(x^*, y^*)}{N_{AB}^*}; \qquad N_S = \frac{N_S^*}{\lambda_D N_{AB}^*};$$

$$N_e = \frac{N_e^*}{\lambda_D N_{AB}^*}; \qquad \varepsilon = \frac{\varepsilon_{Ox}^*}{\varepsilon_{Si}^*}, \tag{11}$$

the normalized differential equations to be solved become

$$\nabla^2 \phi = 0, \qquad y \geq 0; \tag{12}$$

$$\nabla^2 \phi = -\rho(x, y), \qquad y \leq 0, \tag{13}$$

with

$$\rho(x, y) = e^{-\phi} - N_A(x, y) + \delta(y)[N_S(x) - N_e(x)]. \tag{14}$$

The boundary conditions (8) and (9) become

$$\phi = V_i' \text{ on the } i\text{th electrode,} \quad (15)$$

$$\phi \to 0 \text{ as } (x^2 + y^2)^{\frac{1}{2}} \to \infty. \quad (16)$$

On the silicon-oxide boundary,

$$\phi(x, 0+) = \phi(x, 0-); \quad (17)$$

$$\frac{\partial\phi(x, 0+)}{\partial x} = \frac{\partial\phi(x, 0-)}{\partial x}; \quad (18)$$

$$\varepsilon\left[\frac{\partial\phi(x, 0+)}{\partial y} - \frac{\partial\phi(x, 0-)}{\partial y}\right] = -[N_S(x) - N_e(x)]. \quad (19)$$

Numerical method

Equations (12) through (19) are solved numerically. We begin with an assumed initial charge distribution in the silicon and calculate the surface potential by use of a Green's function. A finite-difference method is then used to calculate the potential distribution, and hence the charge distribution, in the silicon. After the new charge distribution is obtained, the whole process is repeated. The iteration continues until a self-consistent result is obtained.

In normalized systems the Green's function, Fig. 2, which is the potential at position (x, y) due to a unit line charge at position (x', y'), can be obtained by the image method [5] as

$$G_{11}(x, y|x', y') = -\frac{1}{4\pi\varepsilon}\left\{\ln[(x-x')^2 + (y-y')^2] - \frac{1-\varepsilon}{1+\varepsilon}\ln[(x-x')^2 + (y+y')^2]\right\},$$
$$y \geq 0,\ y' \geq 0; \quad (20)$$

$$G_{12}(x, y|x', y') = -\frac{1}{4\pi\varepsilon}\left(\frac{2\varepsilon}{1+\varepsilon}\right)\ln[(x-x')^2 + (y-y')^2],$$
$$y \geq 0,\ y' \leq 0. \quad (21)$$

With (20) and (21), the potential at point (x, y) in the upper half-space is given by

$$\phi(x, y) = \sum_{i=1}^{n}\int_{Z_{i,1}}^{Z_{i,m}} q_i(x')G_{11}(x, y|x', h_i)dx' + \int_{-\infty}^{0}\int_{-\infty}^{\infty}\rho(x', y')G_{12}(x, y|x', y')dx'dy', \quad (22)$$

where $q_i(x)$ is the charge distribution on the ith electrode and $Z_{i,m} - Z_{i,1}$ is the width of the ith electrode. If the charge distribution in the silicon is known, the electrode charge distribution can be obtained by requiring that (22) be satisfied, or by solving the following integral equations:

$$V_j' = \phi(x, h_j) = \sum_{i=1}^{n}\int_{Z_{i,1}}^{Z_{i,m}} q_i(x')G_{11}(x, h_j|x', h_i)dx' + \int_{-\infty}^{0}\int_{-\infty}^{\infty}\rho(x', y')G_{12}(x, h_j|x', y')dx'dy',$$
$$Z_{j,1} \leq x \leq Z_{j,m}; \quad j = 1, 2, \cdots, n. \quad (23)$$

Equation (23) cannot be solved analytically. To solve it numerically, we approximate the electrode charge distribution by a piecewise-linear distribution:

$$q_i(x) = \sum_{k=1}^{m-1}\left[q_{i,k} + \frac{q_{i,k+1} - q_{i,k}}{Z_{i,k+1} - Z_{i,k}}(x - Z_{i,k})\right] \times \left[H(Z_{i,k+1}) - H(Z_{i,k})\right],\ i = 1, 2, \cdots, n, \quad (24)$$

where $H(x)$ is the Heaviside step function. Substituting (24) into (23) and requiring that (23) be satisfied at points $(Z_{j,l}\ h_j)$, $l = 1, 2, \cdots, m$, we obtain

$$V_j' - \int_{-\infty}^{0}\int_{-\infty}^{\infty}\rho(x', y')G_{12}(Z_{j,l}, h_j|x', y')dx'dy' = \sum_{i=1}^{n}\sum_{k=1}^{m} q_{i,k}A_{jl,ik},$$
$$j = 1, 2, \cdots, n; \quad l = 1, 2, \cdots, m, \quad (25)$$

where

$$A_{jl,ik} = (1 - \delta_{k1})\int_{Z_{i,k-1}}^{Z_{i,k}}\left(\frac{x' - Z_{i,k-1}}{Z_{i,k} - Z_{i,k-1}}\right) \times G_{11}(Z_{j,l}, h_j|x, h_i)dx' + (1 - \delta_{km})\int_{Z_{i,k}}^{Z_{i,k+1}} 1 - \left(\frac{x' - Z_{i,k}}{Z_{i,k+1} - Z_{i,k}}\right) \times G_{11}(Z_{j,l}, h_j|x', h_i)dx'. \quad (26)$$

The function δ_{km} is the Kronecker delta function. The mn simultaneous linear equations (25) have mn unknown $q_{i,k}$, which can be easily solved if $\rho(x, y)$ is known. After the electrode charge distribution is determined, (24) is substituted back into (22) with $y = 0$ to obtain the surface potential distribution.

In the silicon region, (13) and (14) are solved by the finite-difference method. The lower half-space is superimposed on a grid system, as shown in Fig. 3. Equation (13) is approximated by its finite-difference form,

$$\frac{2}{l_i + l_{i+1}}\left[\left(\frac{\phi_{i+1,j} - \phi_{i,j}}{l_{i+1}}\right) - \left(\frac{\phi_{i,j} - \phi_{i-1,j}}{l_i}\right)\right] + \frac{2}{k_j + k_{j+1}}\left[\left(\frac{\phi_{i,j+1} - \phi_{i,j}}{k_{j+1}}\right) - \left(\frac{\phi_{i,j} - \phi_{i,j-1}}{k_j}\right)\right] = -\rho_{i,j} = -\left[e^{-\phi_{i,j}} - N_A(x_i, y_j)\right] \quad (27)$$

at grid point (x_i, y_j), where

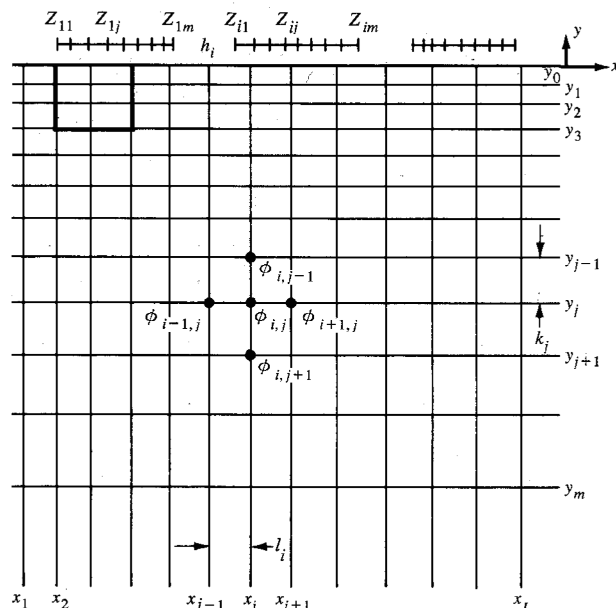

Figure 3 Grid system of the substrate.

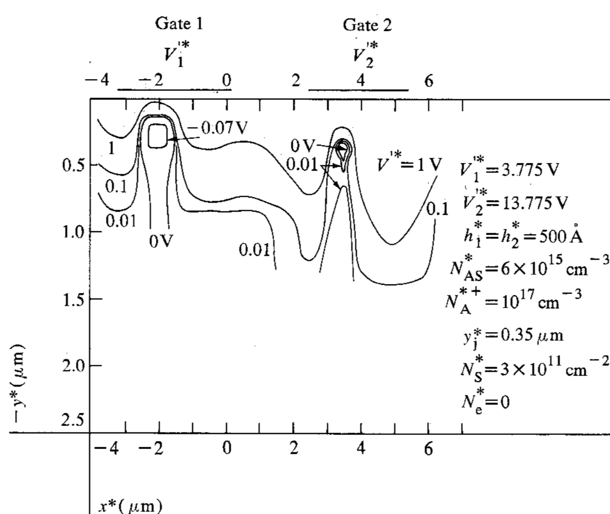

Figure 4 Equipotential contour of a two-electrode MIS array.

$$\phi_{i,j} = \phi(x_i, y_j);$$
$$l_i = x_i - x_{i-1};$$
$$k_j = y_j - y_{j-1}. \tag{28}$$

The previously calculated surface potential distribution is used as a boundary condition of (13). The semi-infinite lower half-space is approximated by a large rectangular region bounded by $x = x_1$, $x = x_L$, $y = 0$, and $y = y_m$. The boundary is chosen large enough so that the region outside of it is neutral when the voltage is applied, or

$$\phi(x_1, y) = \phi(x_L, y) = \phi(x, y_m) = 0;$$
$$\rho = 0; \qquad y \le y_m;\ x \ge x_L;\ x \le x_1. \tag{29}$$

Successive over-relaxation is used to solve (27). After the potential distribution is obtained, the silicon surface potential is refined using the new silicon charge distribution. The iteration continues until a preset criterion is reached for the surface potential. When substituting the new surface potential to calculate the new silicon potential distribution, an under-relaxation and a judicious selection of initial surface potential are required over the region far away from the electrodes and the surface charge. The reason for this is that these potentials are very sensitive to the overall charge imbalance during the iteration. The overall charge converges to zero eventually. Elsewhere a direct substitution is made. The convergent property of the method is not investigated here, but the method usually converged within ten iterations of surface potential for the cases computed.

The integrals in (26) can be evaluated analytically [5]. The double integrals in (22) and (25) are evaluated numerically. A trapezoidal rule is used in the y' integration. In the x' integration, all charge distributions along the x' direction are approximated by piecewise-linear distributions with exact $\rho_{i,j}$ at (x_i, y_j). The resultant integrals can be evaluated analytically. The same approximation applies also to the integrations involving N_S and N_e.

Numerical results

The above formulation takes into acount not only the effect of depletion of majority carriers on the surface, but also any accumulation-depletion phenomenon of the majority carriers due to the inhomogeneity of the substrate. The built-in potential of any high-low junction is automatically calculated. Based on this approach, the typical equipotential contour and the surface potential profile in the absence of externally introduced charges are shown in Figs. 4 and 5, respectively. The maximum allowable injected signal charge level is then limited by the difference between the surface potential of the deep well D under gate 2 and the backflow barrier height A at the p^+ region under gate 1. The electrodes are 3 μm in width and are separated by 2.5 μm. The effective surface charge density, 3×10^{11} e cm^{-2}, where e is the electron charge and will be set to one hereafter for simplicity, is assumed to exist uniformly from −3.5 to 6 μm, i.e., along the entire length of the two adjacent MIS capacitors and the interelectrode region. The heavily doped regions under the metal electrodes extend in the y^* direction to a junction depth y_j^* from −2.5 μm to 1.5 μm and from 3 μm to 4 μm and are doped uniformly to a depth of 0.35 μm. The net charge distribution in the absence of signal charges is shown in Fig. 6. The heavily doped region under gate 2, which has a higher voltage applied than

that for gate 1, is almost completely depleted, whereas that under gate 1 is only partially depleted. The majority carriers can be seen to deplete and then to accumulate across the p^+-p junction.

To have an efficient information-bearing charge (electron) transfer, any accumulation of holes near the surface along the channel has to be prevented, because the information can be degraded through electron-hole recombinations. In the example shown here, the surface of the p^+ region under gate 1 is depleted, and the corresponding depletion width is still larger than the channel depth within which the electron transfer takes place. If the undepleted region lies inside the electron channel depth, a higher applied potential must be used to increase the depletion region and to prevent electron-hole recombinations.

The surface potential distributions of the same device with two effective interface charge densities are shown in Fig. 5. For the effective charge density of 10^{11} cm^{-2}, the interelectrode potential barrier B is higher than barrier A due to the heavily doped region under gate 1. The minority carriers in this case cannot be transferred completely to the gate 2 region. To decrease the barrier the effective surface charge density must be kept high. On the other hand, for the device to be compatible with MOSFET technology, the surface charge density must be kept low; thus the interelectrode spacing must be reduced.

Figure 7 shows the surface potential distributions due to different positioning of the heavily doped region under the gate electrodes. When the heavily doped region lies partially outside the gate region, the barrier cannot be manipulated effectively by the applied voltage. To lower the barrier potential effectively with an applied voltage, these heavily doped regions must be kept inside the gates.

Another application of the analysis is to estimate the isolation between adjacent charge-coupled device channels. The effect of interelectrode doping on the interelectrode potential barrier is shown in Fig. 8. For the phase voltages, oxide thickness, and interelectrode spacing shown in the figure, the interelectrode space acts as an isolator between the two electrodes with a doping density of 10^{17} cm^{-3}. If the doping density is reduced, the barrier is reduced. The amounts of barrier lowering due to different doping thicknesses are also shown in Fig. 8

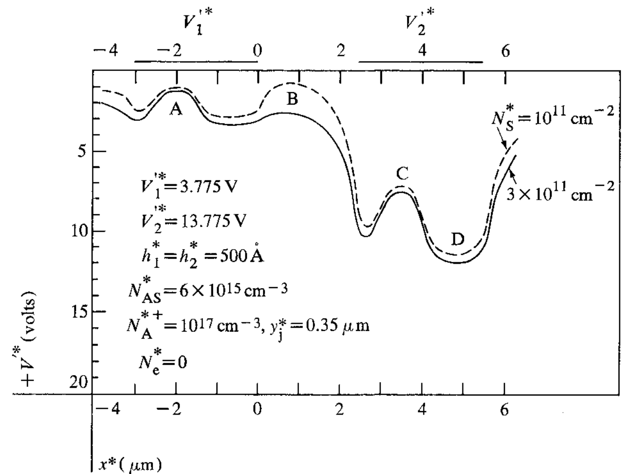

Figure 5 Effect of surface charge on surface potential distribution.

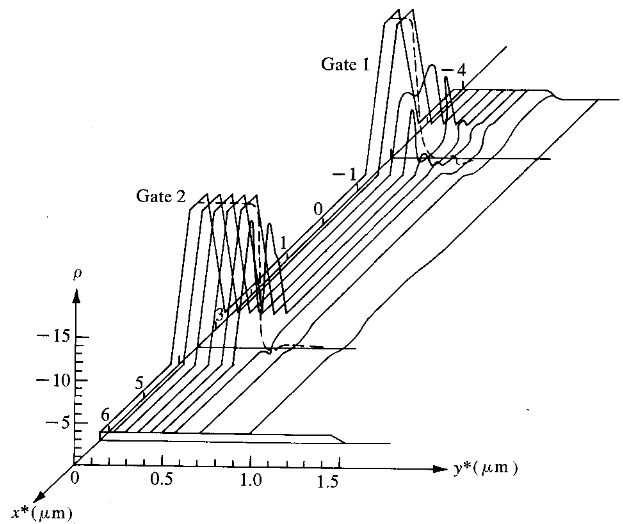

Figure 6 Net charge distribution of the two-element MIS array shown in Fig. 4.

Summary
The numerical method used to obtain the potential distribution of a two-dimensional inhomogeneously doped MIS array under pulse voltage operation has been described. The mathematical model takes into account both the effect of accumulation-depletion of majority carriers on the two-dimensional high-low junction and the effect of depletion of majority carriers on the surface. The analytic method can be readily used for designing a suitable potential profile for a charge transfer device and to determine the isolation between MIS arrays.

References

1. R. H. Krambeck, R. H. Walden and K. A. Pickar, "Implanted-Barrier Two-Phase Charge-Coupled Device," *Appl. Phys. Letters* **19**, 520 (1971).
2. J. A. Magowan, W. D. Ryan and A. Armstrong, "Determination of Laplace-Poisson Domain Interface within Semiconductor Devices," *Proc. IEEE* **117**, 921 (1970).
3. E. Wasserstrom and J. McKenna, "The Potential Due to a Charged Metallic Strip on a Semiconductor Surface," *Bell Syst. Tech. J.* **49**, 853 (1970).

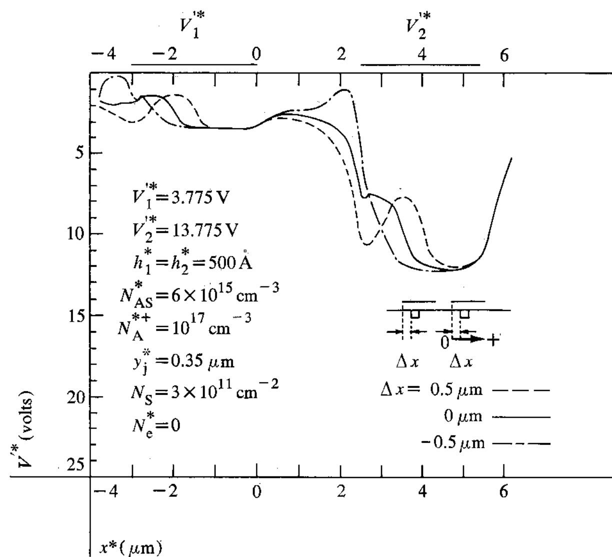

Figure 7 Effect of location of the heavily doped region on surface potential distribution.

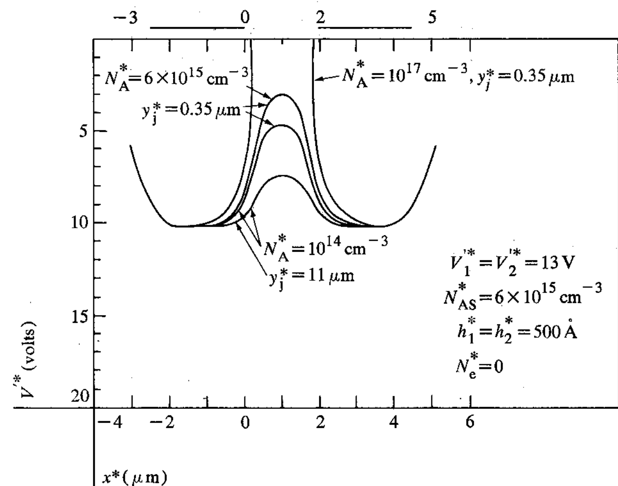

Figure 8 Effect of interelectrode doping density on surface potential distribution.

4. D. P. Kennedy and R. R. O'Brien, "Computer-Aided Two-dimensional Analysis of the Junction Field-effect Transistor," *IBM J. Res. Develop.* **14**, 95 (1970).
5. W. H. Chang, "MIS Array Potential Calculation," *Solid-State Electronics* **16**, 491 (1973).
6. S. R. Hofstein and G. Warfield, "Physical Limitations on the Frequency Response of a Semiconductor Surface Inversion Layer," *Solid-State Electronics* **8**, 321 (1965).

Received March 22, 1973; revised June 15, 1973

The authors are located at the IBM System Products Division, Burlington Laboratory, Essex Junction, Vermont 05452.